PERGAMON

International Journal of Heat and Mass Transfer 43 (2000) 1425–1437

International Journal of HEAT and MASS TRANSFER

www.elsevier.com/locate/ijhmt

Transient, three-dimensional heat transfer model for the laser assisted machining of silicon nitride: II. Assessment of parametric effects

Jay C. Rozzi[a,*], Frank P. Incropera[b], Yung C. Shin[a]

[a]*Laser Assisted Materials Processing Laboratory, School of Mechanical Engineering, Purdue University, USA*
[b]*Aerospace and Mechanical Engineering Department, University of Notre Dame, USA*

Received 5 August 1998; received in revised form 25 June 1999

Abstract

In a companion paper (J.C. Rozzi, F.E. Pfefferkorn, F.P. Incropera, Y.C. Shin, Transient, three-dimensional heat transfer model for the laser assisted machining of silicon nitride: I. Comparison of predictions with measured surface temperature histories, International Journal of Heat and Mass Transfer 43 (2000) 1409–1424), experimental validation was provided for a transient, three-dimensional heat transfer model of the LAM of a silicon nitride workpiece. In this paper, the model is used to elucidate the influence of operating parameters on thermal conditions within the workpiece. Calculations reveal that thermal energy generation in the primary shear zone has a significant influence on the workpiece temperature distribution, while the effects of heat transfer at the tool flank interface may be neglected. Although temperatures at the material removal plane were only moderately influenced by an increase in the workpiece rotational speed, a reduction in total laser energy deposition due to increased laser/tool translational velocity or decreased laser power may preclude the attainment of a minimum material removal temperature corresponding to the softening temperature range of the YSiAlON glassy phase. Due to the comparatively small influence on radial temperature gradients within the material removal plane, the minimum material removal temperature decreased only slightly with increasing depth of cut. However, the amount of laser energy deposition on the unmachined workpiece increased significantly with increasing laser-tool lead distance, yielding an attendant increase in the material removal temperature. For a fixed laser-tool lead, energy deposition at the unmachined workpiece surface increased with decreasing laser beam diameter and increasing power.

1. Introduction

Advanced materials are increasingly being employed in many engineering systems, with ceramics used for components such as mechanical seals and bearings in both internal combustion and gas turbine engines. While such applications are growing, there has not been commensurate improvement in the ability to precisely and rapidly machine these materials. For structural ceramics, finish machining is necessary because of the distortion, contraction, limited formability, and lack of dimensional control achieved in net-shape manufacturing processes [1]. Grinding and diamond

* Corresponding author. Creare, Inc., P.O. Box, Hanover, NH 03755, USA. Tel.: 1-603-643-3800; fax: 1-603-643-4657.
E-mail address: jcr@creare.com (J.C. Rozzi).

0017-9310/00/$ - see front matter
PII: S0017-9310(99)00219-7

Nomenclature

d	depth of cut, m
D	diameter, m
h	heat transfer coefficient, W/m^2 K
L_f	tool feed in single point machining, m
L_ℓ	laser-tool lead distance, m
Nu	Nusselt number
P	power, W
q_{flank}	heat generated due to friction at the cutting tool flank which is conducted into the workpiece, W
q_{pl}	heat generated due to plastic deformation in the primary shear zone, W
r	radius, m
r_w	workpiece radius, m
S_{psz}	thickness of the primary shear zone, m
t	time, s
t_p	preheat time, s
T	temperature, K
T_{max}	maximum temperature on the workpiece surface, K
T_{mr}	temperature at the material removal plane, K
$T_{mr,min}$	minimum temperature at the material removal plane, K
V_z	laser/tool translational velocity, m/s
z	axial coordinate, m
z_c	axial location of the laser center, m
$z_{fe,o}$	initial axial location of the workpiece free end, m

Greek symbols

α_ℓ	absorptivity of the unmachined (sintered) workpiece surface to irradiation from the CO_2 laser
$\alpha_{\ell,m}$	absorptivity of the machined workpiece surface to irradiation from the CO_2 laser
ε	emissivity of the unmachined (sintered) workpiece surface; strain
ε_m	emissivity of the unmachined (sintered) workpiece surface
ϕ	circumferential coordinate, rad
ϕ_c	circumferential location of the laser center, rad
ϕ_{lank}	circumferential extent of flank wear region for single point machining, rad
ϕ_ℓ	circumferential distance between the laser center location and the material removal plane, rad
ν	workpiece rotational speed, rpm
ω	workpiece rotational speed, rad/s

Subscripts

c	source geometric center
j	laser gas assist jet
ℓ	laser beam
max	maximum
min	minimum
mr	material removal plane

machining currently provide the only processing options [2,3] and represent as much as 60–90% of the final product cost. Although laser evaporation has been proposed as a material removal process [4], surface micro-cracking and altered material composition are present in the heat-affected zone. Alternatively, in a hybrid, laser assisted machining (LAM) process, the material is subjected to intense heating just before it is machined, thereby changing the material deformation behavior from brittle to ductile (without melting or sublimation) and providing for material removal by plastic deformation. Once fully developed, the LAM process is expected to yield higher material removal rates, reduced man and machine hours per part, an increased ability to precisely control part geometry, and substantial cost savings.

Although the effectiveness of LAM has been demonstrated [1], underlying physical mechanisms are not well understood, and a comprehensive thermo-mechanical model of the heating and material removal processes is needed to facilitate optimization and intelligent control of the process. Several thermal processes occur simultaneously during LAM and may influence the development of a control scheme. They include: (1) laser irradiation and sub-surface conduction of the absorbed heat flux, (2) convection heat transfer from the rotating workpiece to the ambient air and to an impinging jet known as the laser gas assist, (3) emission from the workpiece to the surroundings, (4) radial, axial, and circumferential conduction through the workpiece, (5) energy advection out of the system with the heated chips, (6) thermal energy generation associated with plastic work, and (7) frictional heating and conduction heat transfer at the chip–tool interface.

Analytical and semi-analytical solutions for the problem of conduction heat transfer in a rotating cylinder have yielded two-dimensional, steady-state temperature fields for various surface heat flux distributions, with applications to cold and hot rolling of strip steel, as well as laser hardening [5–9]. However, in these studies, the heat equation did not include z-advection or

z-conduction terms, which along with energy storage effects, can significantly influence the transient temperature distribution for a moving heat source.

Use of non-dimensional calculations and a scaling analysis [10] to assess transient, three-dimensional thermal conditions within a rotating cylinder subjected to a translating laser source have revealed that: (1) with increasing workpiece rotational speed or laser translational velocity, there is a greater concentration of thermal energy near the surface of the workpiece, a reduction of conduction into the workpiece, and a decrease in the maximum temperature on the workpiece surface; (2) conduction in the axial direction has a significant effect on the quasi-steady temperature distribution, particularly for small values of the translational velocity; and (3) surface mixed convection and radiation effects are negligible.

A later study [11] utilized a transient, three-dimensional numerical simulation to predict the thermal response of a rotating silicon nitride workpiece to irradiation by an axially translating laser. The model, which included temperature-dependent thermophysical properties and treatment of convective heat transfer to a laser gas assist jet, yielded the following conclusions: (1) the thermal layer thickness for an r–ϕ plane cutting through the center of the laser source decreases with increasing workpiece rotational speed; (2) the influence of heat transfer by conduction in the z-direction increases with decreasing laser traverse velocity; (3) local temperatures increase throughout the workpiece for increasing laser power; and (4) outer region temperatures decrease with increasing beam diameter due to a diminished potential for near-laser conduction heat transfer. It was also found that, while mixed convection to the ambient air and surface emission to the surroundings are negligible, forced convection associated with the gas assist jet and temperature-dependent thermophysical properties can significantly influence the maximum surface temperature beneath the laser spot. An approximate model was also developed [11], and predictions were generally in good agreement with those based on the more detailed numerical simulation, particularly in a near-surface region corresponding to the maximum depth of cut. This model provided a useful, simplified tool for assessing the effect of operating conditions on the sub-surface temperature distribution, for establishing preferred process operating conditions, including cutting tool placement, and most importantly, for on-line process control.

The foregoing studies involved laser heating without material removal (machining). In contrast, using the three-dimensional heat transfer model described by Rozzi et al. [12], the present study seeks to clarify the role of physical phenomena associated with LAM and,

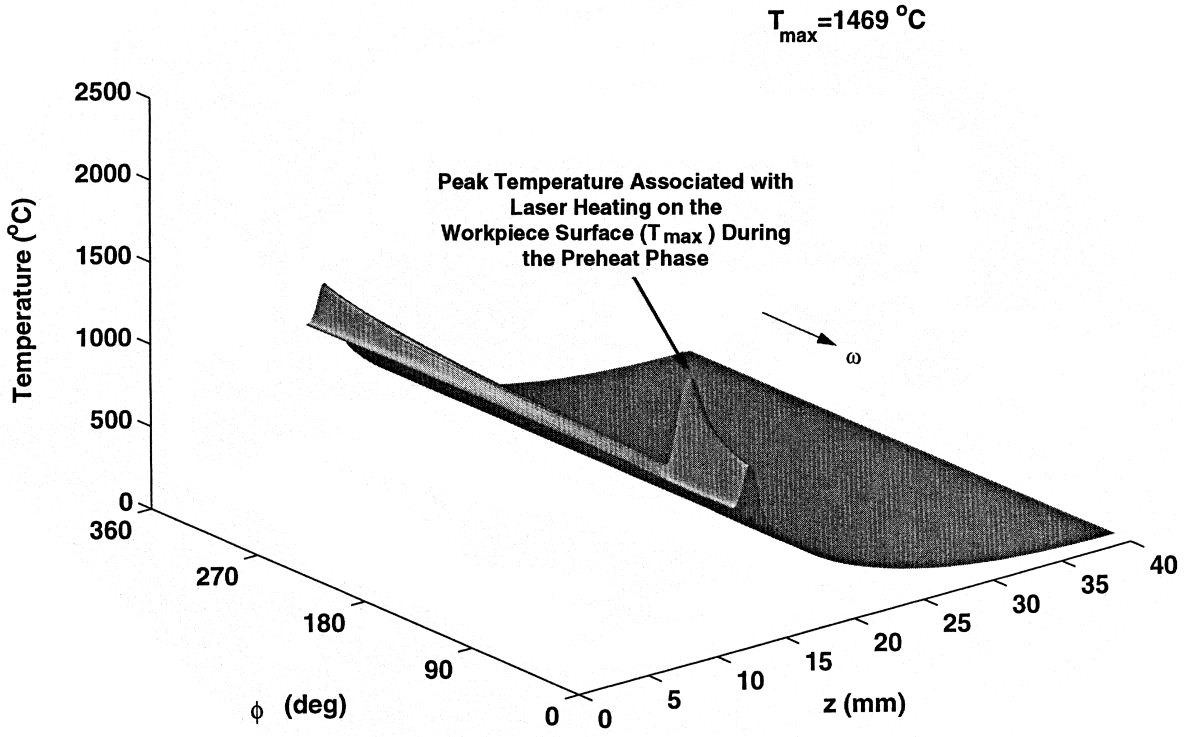

Fig. 1. Predicted ϕ–z surface ($r = r_w$) temperature distribution at the end of the preheat phase ($t = 10$ s) for Case 1.

in particular, to determine the influence of operating conditions on the temperature distribution within the heated workpiece and near the region of material removal.

2. Numerical results

Calculations were completed for operating conditions corresponding to the LAM experiments and are listed in Table 1 of the companion paper [12]. The coordinate system for the computations corresponds to that of Fig. 2 in the companion paper [12], and results are presented in terms of three-dimensional plots of the surface temperature distribution and two-dimensional (ϕ–z, r–z) temperature contours. The circumferential distance between the laser center location, ϕ_c, and the material removal plane, located at $\phi = 0°$, corresponds to that used in the experimental study ($\phi_c = \phi_\ell = 55°$), and the axial location of the laser center corresponds to $z_c = 12.67$ mm. Because the coordinate system is fixed relative to the laser source, ϕ_c and z_c remain constant for the duration of the computation. During the preheat phase, the free end of the workpiece was located at $z_{fe,o} = 11$ mm and, as illustrated in Fig. 1 of Rozzi et al. [12], decreased with movement of the workpiece in the negative z-direction after initiation of material removal.

At the conclusion of the preheat phase ($t = 10$ s), the ϕ–z surface temperature distribution in proximity to the laser source is strongly influenced by conduction in all coordinate directions, as evidenced by the large near-laser temperature gradients in Fig. 1. The maximum surface temperature corresponds to intense heating at the laser center, but temperatures and circumferential temperature gradients decrease significantly with increasing z. For $z \approx z_c + 6$ mm, the influence of conduction yields a surface temperature distribution which is circumferentially uniform to within 5°C.

Upon the initiation of material removal, the chamfer, as illustrated by Fig. 2 of Ref. [12], is established along a helical plane defined by the line extending from the (ϕ, z) location (0°, 12.2796 mm) to (360°, 12.2896 mm), corresponding to a tool feed, L_f, of 0.01 mm, and extending to a depth d below the unmachined workpiece surface. Thus, control volumes associated with the region from $r_w - d$ to r_w and having z-locations less than those associated with the chamfer do

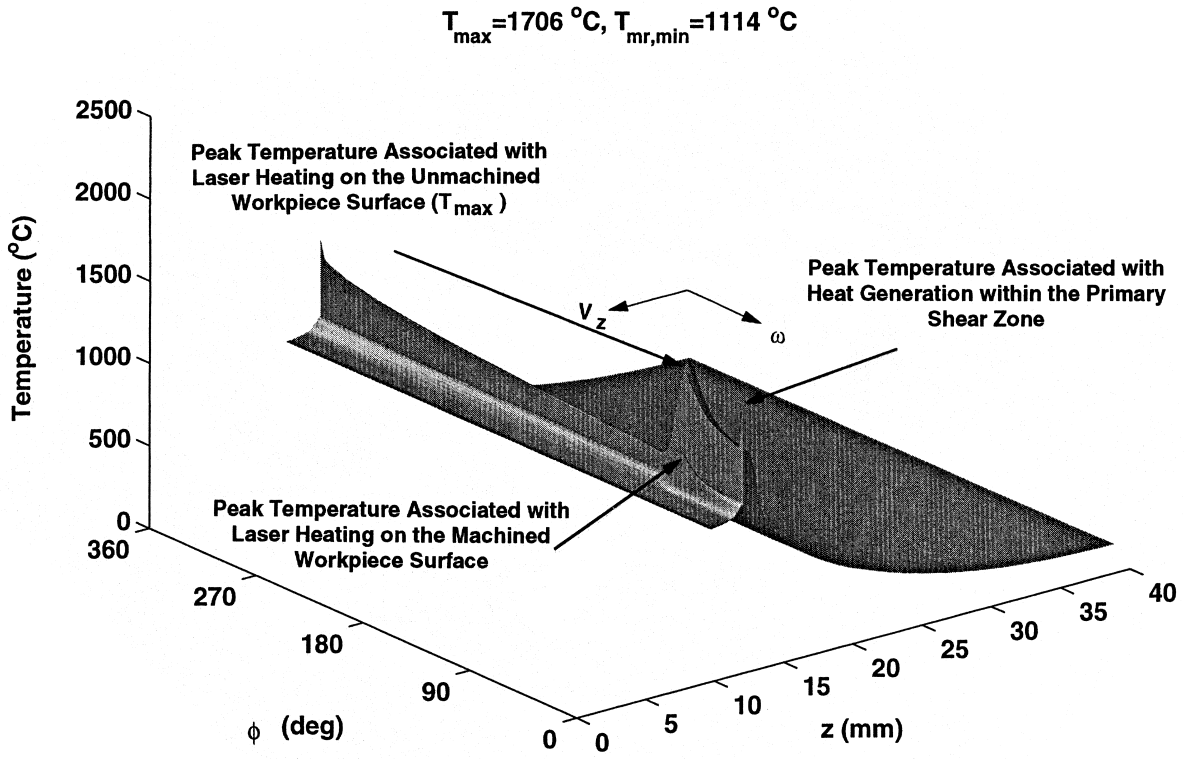

Fig. 2. Predicted ϕ–z machined ($r = r_{w,m}$) and unmachined ($r = r_w$) surface temperature distribution during material removal at $t = 20$ s for Case 1.

not participate in heat transfer by conduction or advection upon initiation of material removal. The material removal plane, as displayed by the inset of Fig. 2 of Ref. [12], is located within a region defined by $12.2796 \le z \le 12.2896$ mm and $r_w - d \le r \le r_w$ at $\phi = 0^\circ$.

For the nominal conditions, the laser overlaps the chamfer interface by approximately 0.865 mm, as measured along a line extending in the z-direction and originating at the laser center location. Thus, approximately 28% of the laser spot is incident upon the machined workpiece surface and, because the absorptivity of the machined surface at the wavelength of laser irradiation ($\alpha_{\ell,m} \approx 0.36$) is significantly less than that associated with the sintered, unmachined workpiece surface ($\alpha_\ell \approx 0.83$), the peak temperature of the machined surface is significantly less than that of the unmachined surface. This condition is illustrated in Fig. 2, which reveals the surface temperature distribution 10 s after the start of machining. For a laser/tool translational velocity of $V_z = 10$ mm/min, the workpiece free end has extended 1.67 mm in the negative z-direction, and maximum temperatures associated with the unmachined and machined surfaces are 1706 and 1160°C, respectively. The influence of conduction within the machined workpiece has rendered the surface temperature distribution circumferentially uniform to within 4°C for z-locations corresponding to $(z_c - z) > 1.2$ mm. Thermal energy generation in the primary shear zone provides a significant local maximum in the surface temperature (1670°C) near the material removal plane at $\phi = 0^\circ$. While most of the generated thermal energy added by plastic deformation is transferred by advection in the circumferential direction, redistribution also occurs by conduction in all coordinate directions. There is a significant increase in T_{max} relative to that associated with the preheat phase (Fig. 1), which persists throughout the LAM process. This continuous increase in the maximum temperature suggests that quasi-steady conditions are not achieved, and the entire process must be characterized as time-dependent. While the minimum temperature at the material removal plane ($T_{mr,min}$) occurs at radial locations corresponding to the depth of cut ($r \approx r_w - d$), its value is indicated in Fig. 2 for reference.

The foregoing trends continue as machining progresses to $t = 60$ s (Fig. 3), at which time the free end of the workpiece has moved a distance of 8.33 mm. Values of T_{max} and $T_{mr,min}$ continue to increase during this period, but at decreasing rates, suggesting that quasi-steady conditions are being approached asympto-

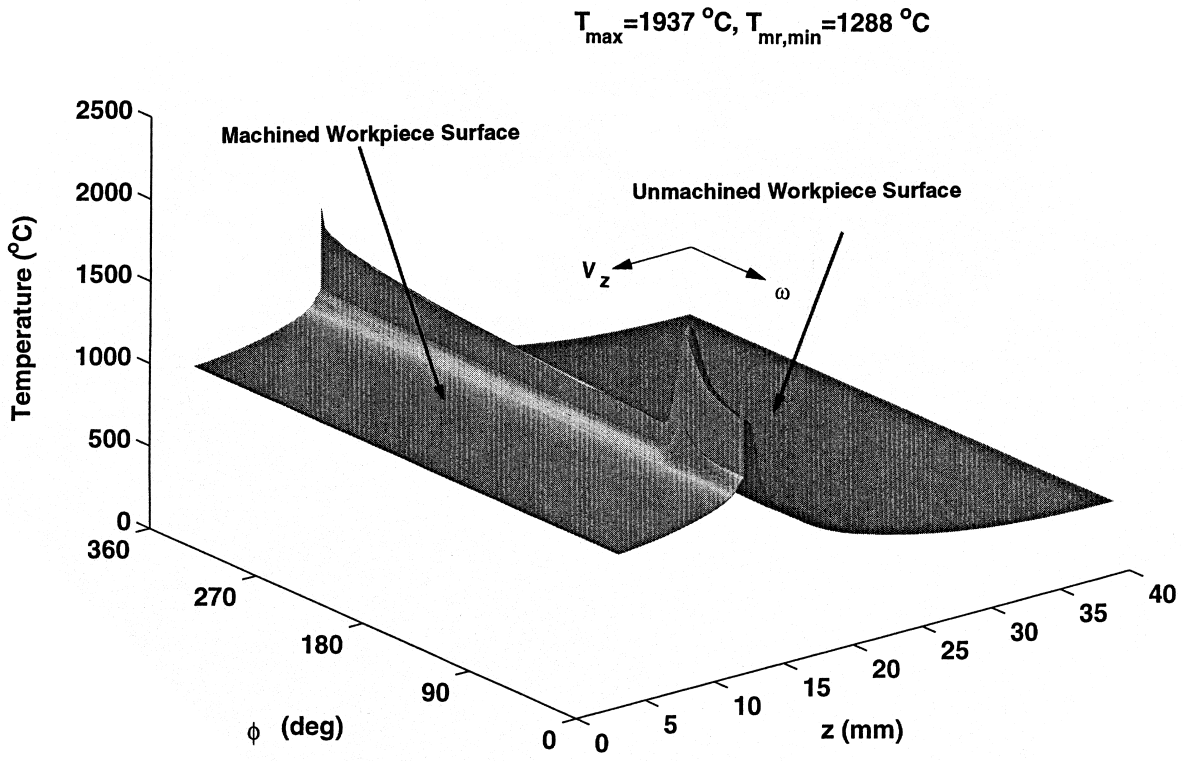

Fig. 3. Predicted ϕ–z machined ($r = r_{w,m}$) and unmachined ($r = r_w$) surface temperature distribution for Case 1 at $t = 60$ s during material removal.

tically. The peak unmachined surface temperature associated with heat generation in the primary shear zone also increases at a decreasing rate to 1904°C from a value of 1670°C at $t = 20$ s. The unmachined workpiece surface temperature distribution at $t = 60$ s is circumferentially uniform to within 8 and 0.1°C at $z \approx z_c + 6$ mm and $z \approx z_c + 12$ mm, respectively, due to the influence of conduction and circumferential advection. On the machined workpiece surface, the temperature distribution is circumferentially uniform to within 5°C for $(z_c - z) > 1.2$ mm.

To gain insight regarding the transport of thermal energy within the workpiece, temperature contours within r–z planes located at $\phi = 55°$ and $\phi = 0°$, which correspond to sections cutting through the laser center and the plane of material removal, respectively, are presented in Fig. 4 at $t = 40$ s, along with the ϕ–z surface temperature contours. Rotation of the workpiece away from the laser source results in decreased machined and unmachined surface temperatures and temperature gradients due to radial and axial conduction (Fig. 4(a)). Beneath the laser source (Fig. 4(b)), significant near-surface radial and axial temperature gradients exist in the unmachined workpiece, and for increasing $z > z_c$ the temperature distribution is increasingly one-dimensional, with axial conduction the dominant mechanism of thermal energy transport. However, negative radial temperature gradients at the unmachined workpiece surface are evident beyond the region coincident with the laser source. The gradients support radial conduction to the surface, which results from the comparatively large convection heat transfer coefficients associated with the gas assist jet ($h_j > 1500$ W/m^2 K). The longer duration of the LAM process ($t \approx 70$ s) compared to laser heating without material removal ($t \approx 9$ s) [12], which did not require a preheat phase, and the correspondingly large temperatures which develop within the machined workpiece also provide discernible surface heat losses due to mixed convection and radiation, as evidenced by the negative radial temperature gradients near the machined surface. In contrast, for z-locations beyond the interaction area associated with the laser gas assist jet, surface temperatures are significantly less than those at the machined workpiece surface, resulting in significantly reduced surface heat losses.

During rotation of the workpiece in the negative ϕ-direction, there is increased radial penetration of the

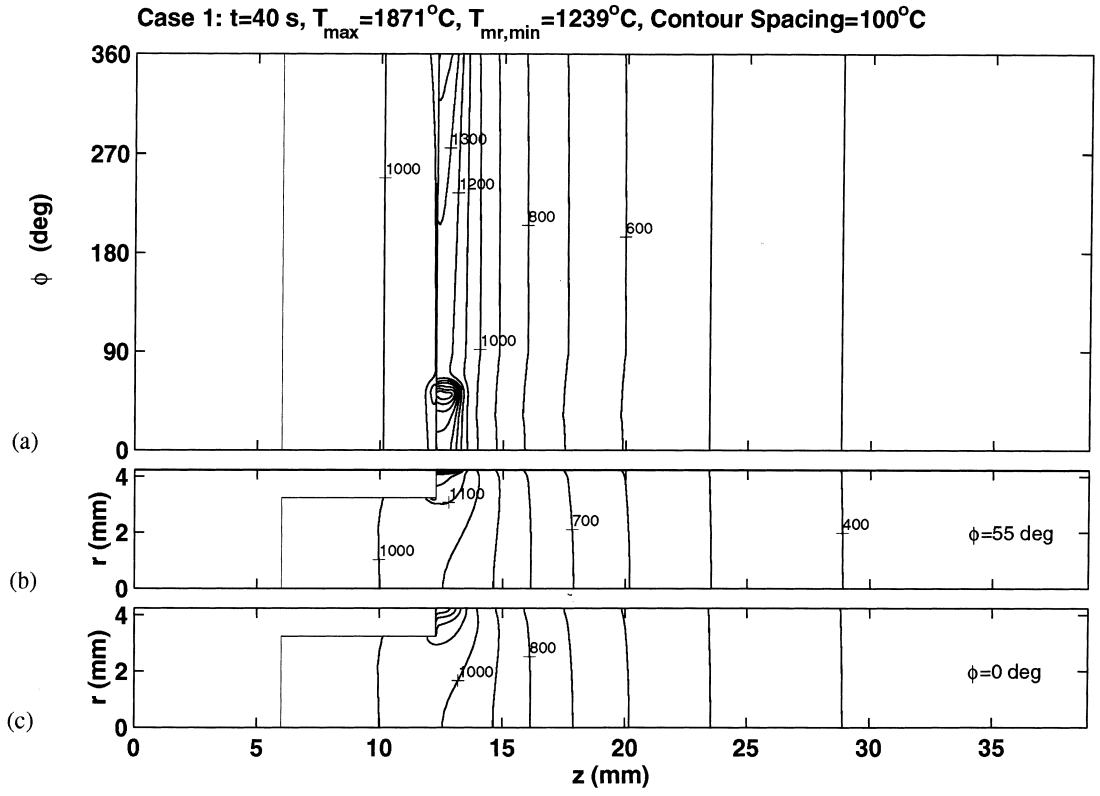

Fig. 4. Predicted (a) ϕ–z machined ($r = r_{w,m}$) and unmachined ($r = r_w$) surface temperature contours and r–z temperature contours at (b) the laser center ($\phi = 55°$) and (c) the material removal plane ($\phi = 0°$) during material removal at $t = 40$ s for Case 1.

deposited laser energy and an attendant surface temperature reduction at the material removal plane ($\phi = 0^\circ$), as evidenced by Fig. 4(c). Heat generation within the primary shear zone has resulted in significant negative z-direction temperature gradients. These gradients support axial conduction into the unmachined workpiece, where the thermal energy is distributed by advection and circumferential/radial conduction.

For axial locations removed from the laser source, the temperature distribution becomes one-dimensional, as illustrated in Fig. 5, which provides the temperature variation in an r–z plane cutting through the laser center ($\phi = 55^\circ$) at $t = 40$ s. Large radial temperature gradients are concentrated near the machined and unmachined workpiece surface locations corresponding to laser heating. In contrast, as the workpiece rotates away from the laser to the material removal plane ($\phi = 0^\circ$), increased radial penetration of deposited thermal energy decreases radial temperature gradients and surface temperatures. The temperature distribution over the material removal plane is axially uniform due to the small tool feed, $L_f = 0.01$ mm. However, radial conduction reduces temperatures along the material removal plane at locations beneath the unmachined workpiece surface, and locations of the maximum and minimum temperature at this plane correspond to $r = r_w$ and $r = r_w - d$, respectively.

2.1. Influence of thermal energy generation due to machining

To investigate the influence of thermal energy generation due to plastic deformation within the primary shear zone and friction at the tool flank on the workpiece temperature distribution, separate calculations were performed for the nominal operating conditions with (1) $q_{pl} = q_{flank} = 0$ W, (2) $q_{pl} = 11$ W and $q_{flank} = 0$ W, and (3) $q_{pl} = 0$ W and $q_{flank} = 4$ W, where the values of $q_{pl} = 11$ W and $q_{flank} = 4$ W were obtained from the cutting force measurements of Ref. [13]. Relative to results for $q_{flank} = 0$ W, heating at the location corresponding to flank wear ($r_w - d < r < r_w$, $358.92^\circ < \phi < 360^\circ$) produces a slight increase (~40°C) in the surface temperature at $\phi = 359.46^\circ$ compared to identical operating conditions without flank wear heating. However, circumferential advection and radial conduction transport this thermal energy about the cylinder circumference and to the workpiece inner region, respectively, and temperatures at the material removal plane ($\phi = 0$) are not significantly affected by

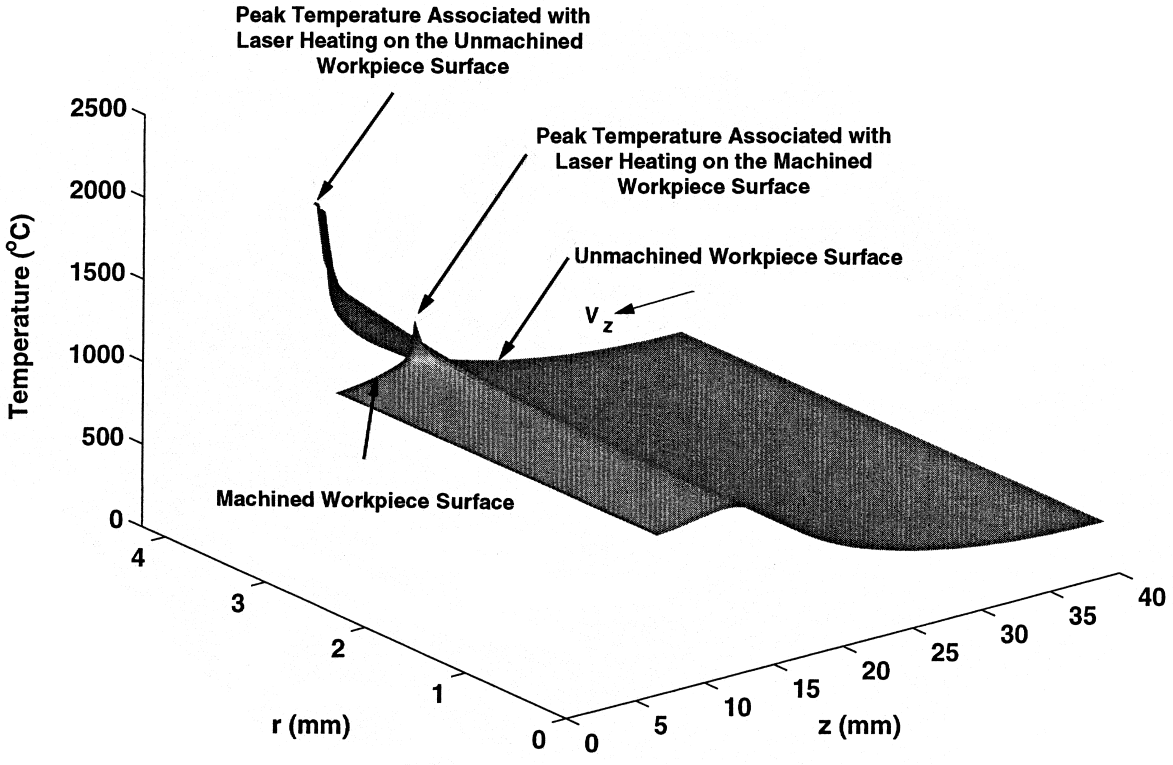

Fig. 5. Predicted r–z temperature distribution beneath the laser center ($\phi = 55^\circ$) during material removal at $t = 40$ s for Case 1.

flank wear heating. During the time required for one rotation of the workpiece (0.06 s) conduction distributes the thermal energy deposited by flank wear heating to inner workpiece regions, and a negligible temperature rise (~5°C) occurs at the location of material removal. Therefore, for the conditions of the present study, flank wear heating does not significantly influence the workpiece temperature distribution.

Due to the small volume of the primary shear zone (~10^{-5} mm^3), there is a significant increase in the surface temperature of the unmachined workpiece at ϕ-locations just prior to the material removal plane (~400°C) compared to predictions which neglect heating in the primary shear zone. While the majority of the generated thermal energy leaves the workpiece with the removed material (chips), axial conduction and circumferential advection transport a portion of this energy into the unmachined workpiece and about the cylinder circumference, respectively. This transport is manifested by a modest (~50–80°C) temperature increase at circumferential locations removed from the primary shear zone along the unmachined workpiece surface at an axial location just beyond that of the chamfer ($z \approx 12.29$ mm). Additionally, uniform heat generation within the primary shear zone results in a nearly uniform temperature rise (~100°C) over the material removal plane compared to predictions with $q_{pl} = 0$ W.

2.2. Assessment of parametric variations

The influence of decreasing workpiece rotational speed, v, on the machined and unmachined workpiece temperature distribution is revealed by contrasting Figs. 4 and 6. As in the case of laser heating without machining [11], circumferential advection decreases with decreasing v, thereby increasing surface temperatures beneath the laser spot and decreasing surface temperatures at circumferential locations far from the laser source in the direction of workpiece rotation. This behavior is seen by contrasting the results of Figs. 4(a) and 6(a). The increased importance of radial conduction relative to circumferential advection is manifested by a slight increase in the radial penetration of the temperature distribution beneath the laser spot (Figs. 4(b) and 6(b)). For a fixed laser/tool translational velocity, the amount of absorbed laser radiation

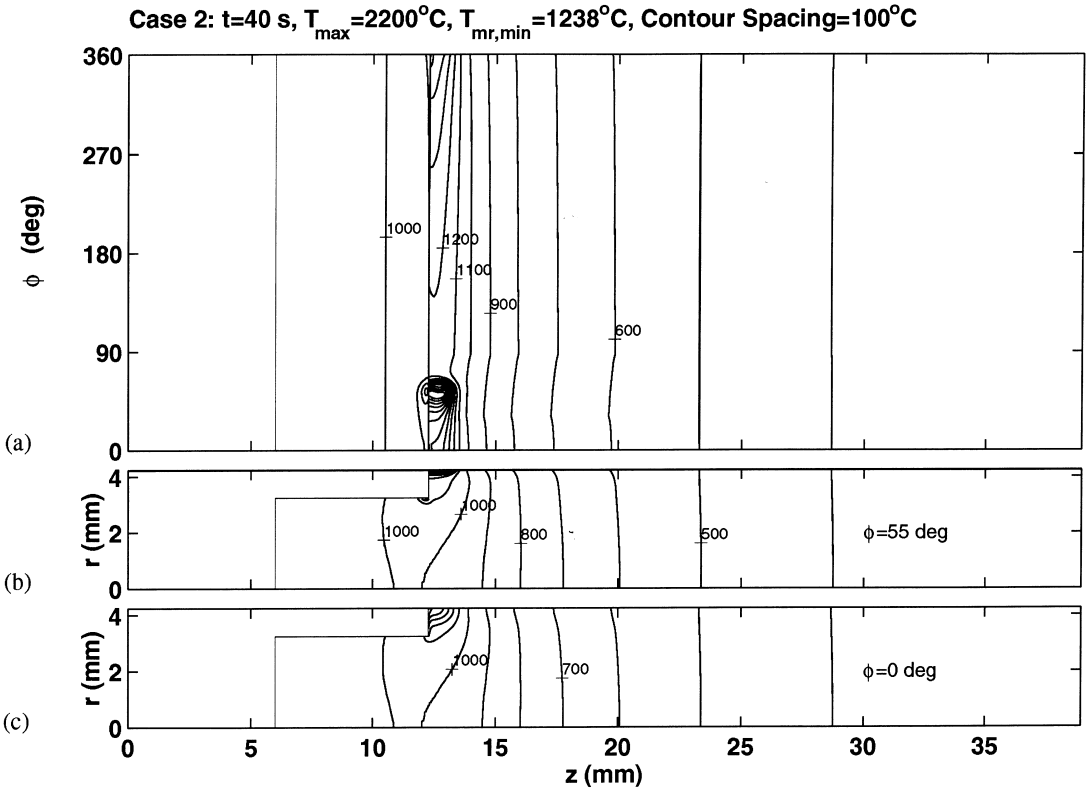

Fig. 6. Predicted (a) ϕ–z machined ($r = r_{w,m}$) and unmachined ($r = r_w$) surface temperature contours and r–z temperature contours at (b) the laser center ($\phi = 55°$) and (c) the material removal plane ($\phi = 0°$) during material removal at $t = 40$ s for Case 2.

remains constant and, hence, at axial locations far from the laser source, the temperature distribution is unaffected by a decrease in v. However, there is a slight increase in the magnitude of the negative axial temperature gradient near the material removal plane (Figs. 4(c) and 6(c)). For a fixed value of the rate of thermal energy generation within the primary shear zone, the portion of this energy which leaves the workpiece decreases with decreasing circumferential advection, thus increasing conduction of generated thermal energy into the unmachined workpiece.

Similar trends are revealed by contrasting results for Case 1 ($v = 1000$ rpm) with those of Case 3 ($v = 2000$ rpm). Circumferential advection increases with increasing workpiece rotational speed, thereby decreasing and increasing temperatures beneath and far from the laser spot, respectively. In addition, the minimum temperature on the material removal plane ($T_{mr,min}$) decreases slightly due to decreasing radial penetration of the temperature distribution. The amount of thermal energy generation due to plastic deformation leaving the system at the material removal plane increases with increasing circumferential advection, thereby reducing the magnitude of the axial temperature gradient which transports thermal energy from the primary shear zone into the unmachined portion of the workpiece.

The duration of machining decreases with increasing laser/tool translational velocity, thereby reducing the amount of laser energy absorbed by the workpiece for a fixed machined length. The effects of V_z may be inferred from Figs. 4 and 7, which correspond to values of 10 and 30 mm/min, respectively. Although temperature gradients within the workpiece are not significantly influenced by V_z, temperatures decrease with increasing V_z due to the decreased laser radiation absorption. Additionally, the reduction of laser radiation absorption may preclude the attainment of a minimum material removal temperature corresponding to the softening temperature range of the YSiAlON glassy phase (920–970°C). Acceptable LAM was completed for $V_z = 20$ mm/min [12], while cutting tool and workpiece fracture resulted from LAM at $V_z = 30$ mm/min [13]. The corresponding minimum material removal temperatures were 1043 and 933°C, which are, respectively, slightly above and near the lower bound of values associated with YSiAlON softening. As axial advection increases, the relative influence of axial conduction within the machined portion of the workpiece

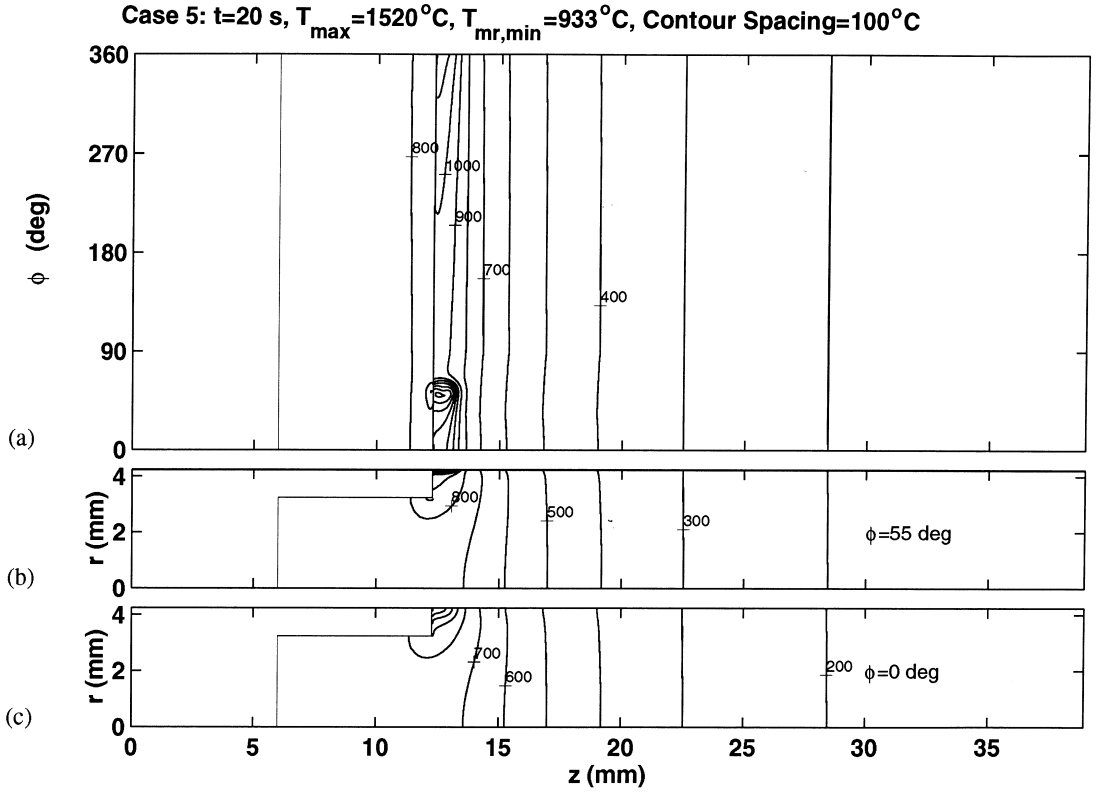

Fig. 7. Predicted (a) ϕ–z machined ($r = r_{w,m}$) and unmachined ($r = r_w$) surface temperature contours and r–z temperature contours at (b) the laser center ($\phi = 55°$) and (c) the material removal plane ($\phi = 0°$) during material removal at $t = 40$ s for Case 5.

decreases, resulting in a nearly uniform temperature distribution.

An increase in the depth of cut from 1 to 1.5 mm does not significantly influence the temperature gradients on the workpiece surface, as illustrated by Figs. 4 and 8(a). However, the 50% increase in the area of the material removal plane increases the thermal energy leaving the system with the heated material, thereby reducing workpiece temperatures, as demonstrated by the decrease in the maximum temperature at the laser spot. This effect is also manifested by a reduction in the minimum material removal temperature. However, the relatively low heat transfer rates associated with mixed convection and emission from the chamfer surface to the ambient air and surroundings, respectively, render the chamfer a significant thermal resistance to heat transfer in the z-direction, compared to similar operating conditions (v, V_z, P_ℓ, D_ℓ) without material removal. The effect of the resistance increases with increasing depth of cut, as demonstrated by the restriction of the 1100°C isotherm to the unmachined portion of the workpiece for $d = 1.5$ mm (Fig. 8(b) and (c) compared to the nominal operating condition (Fig. 4(b) and (c).

A reduction in the laser-tool lead distance decreases energy deposition within the unmachined workpiece, thereby decreasing surface temperatures and temperature gradients. Although more laser radiation is incident on the machined surface, the comparatively low absorptivity of this surface ($\alpha_{\ell,\,\mathrm{m}} = 0.36$), reduces the total rate of laser energy deposition compared to the nominal operating condition. Although advection in the negative z-direction precludes significant transport of energy deposited at the machined surface to the material removal plane, the value of $T_{\mathrm{mr,min}}$ remains large enough to sustain material removal by plastic deformation, and there is little difference in the cutting force and specific cutting energy requirements between Case 1 and Case 7 [13].

If the laser-tool lead distance is increased to $L_\ell = 2$ mm (Fig. 9), the laser no longer overlaps the chamfer. Radial and axial conduction in the near-laser region reduce the surface temperatures of the unmachined workpiece near the chamfer interface (Figs. 4(a) and 9(a)) and increase radial uniformity of the temperature distribution at the chamfer (Figs. 4(b),(c) and 9(b),(c)). Although there is essentially no change in $T_{\mathrm{mr,min}}$, the average temperature over the material removal plane

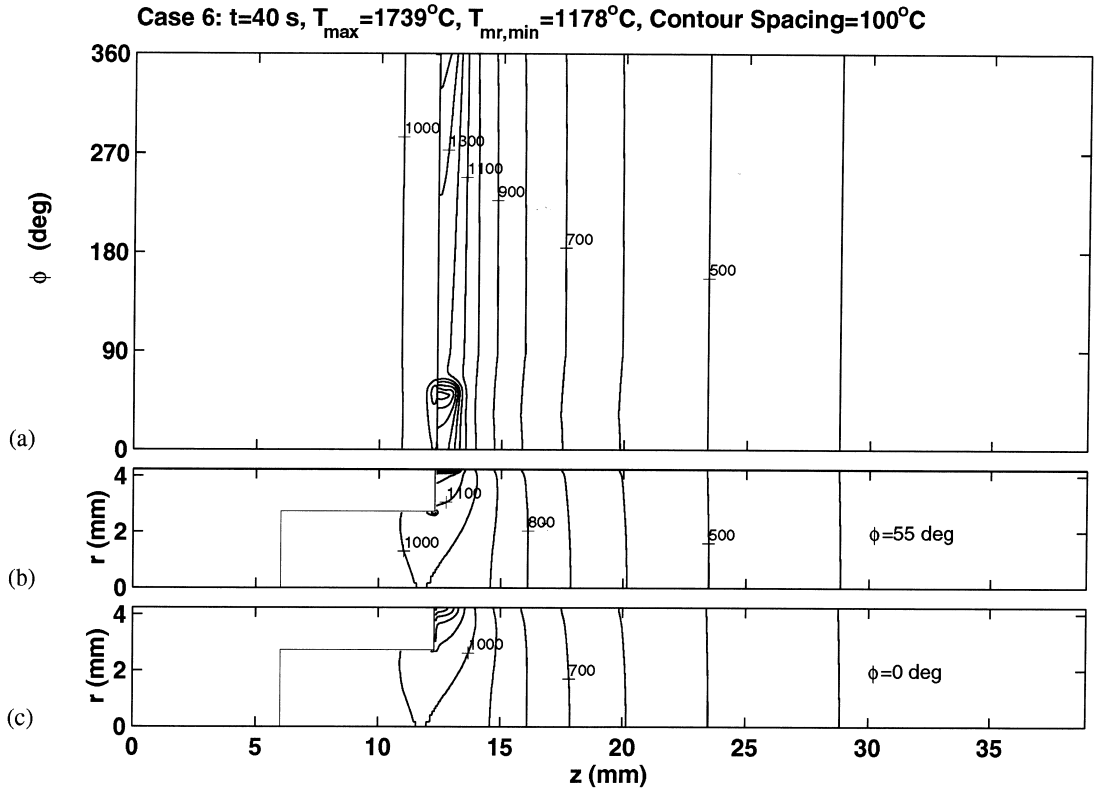

Fig. 8. Predicted (a) ϕ–z machined ($r = r_{\mathrm{w,m}}$) and unmachined ($r = r_{\mathrm{w}}$) surface temperature contours and r–z temperature contours at (b) the laser center ($\phi = 55°$) and (c) the material removal plane ($\phi = 0°$) during material removal at $t = 40$ s for Case 6.

decreases from 1369°C for the nominal conditions, to 1287°C for $L_\ell = 2$ mm. Therefore, the increase in the laser-tool lead distance does not significantly influence the degree of thermal softening, and nearly constant values of the cutting force and the specific cutting energy were obtained over the range $0.6 \leq L_\ell \leq 2$ mm [13].

If the laser-tool lead is fixed, decreasing the beam diameter, D_ℓ, increases laser radiation absorption by the unmachined workpiece surface, as well as heat fluxes beneath the laser spot. Relative to the nominal conditions (Fig. 4), the principal effect is to increase temperatures and temperature gradients on the unmachined surface near (Figs. 4 and 10(a)) and at radial locations just beneath (Figs. 4(b) and 10(b)) the laser source. In addition, there is an increase in temperatures and radial temperature gradients over the material removal plane, particularly near the unmachined workpiece surface (Figs. 4(c) and 10(c)). Far from the laser source, the workpiece temperature distribution is relatively unaffected by a decrease in the laser beam diameter.

In contrast, for a fixed L_ℓ, the increase in D_ℓ associated with Case 10 decreases both the laser radiation incident on the unmachined workpiece surface and heat fluxes beneath the laser spot. This effect is manifested by a reduction in surface temperatures ($T_{max} = 1620$°C at $t = 40$ s) and temperature gradients, as well as in radial penetration of the temperature distribution. Consequently, temperatures and temperature gradients along the material removal plane are reduced ($T_{mr,\,min} = 1175$°C at $t = 40$ s), suggesting a decrease in the degree of thermal softening. This behavior is consistent with experimental results [13]. As in the case of decreasing D_ℓ, increasing the beam diameter had little influence on the workpiece temperature distribution at locations removed from the laser source.

The foregoing numerical results suggest the existence of an optimum value of the beam diameter for a particular laser-tool lead distance. If the beam diameter is too large, a greater percentage of the incident laser radiation will be absorbed by the machined workpiece surface. This effect may degrade the machined surface quality due to a reheating of the YSiAlON glassy phase and increase the cutting forces and the specific cutting energy due to decreased temperatures in the material removal plane. Conversely, if the beam diameter is too small, the increased radial temperature gra-

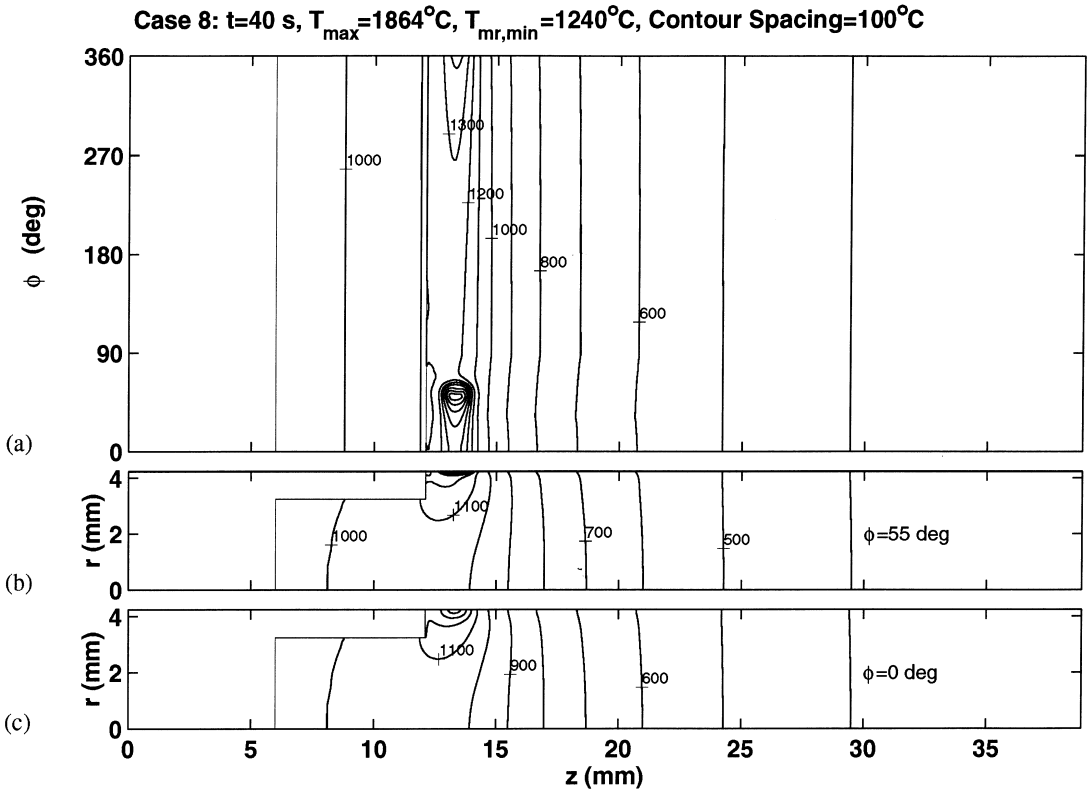

Fig. 9. Predicted (a) ϕ–z machined ($r = r_{w,m}$) and unmachined ($r = r_w$) surface temperature contours and r–z temperature contours at (b) the laser center ($\phi = 55°$) and (c) the material removal plane ($\phi = 0°$) during material removal at $t = 40$ s for Case 8.

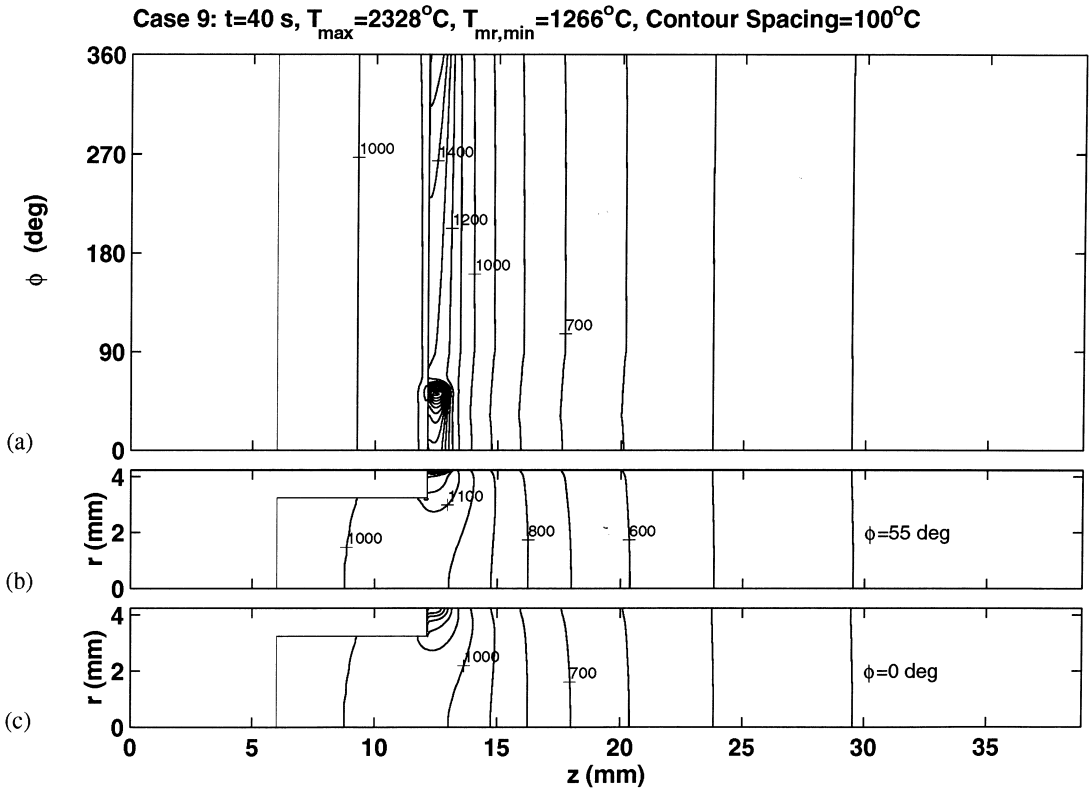

Fig. 10. Predicted (a) ϕ–z machined ($r = r_{w,m}$) and unmachined ($r = r_w$) surface temperature contours and r–z temperature contours at (b) the laser center ($\phi = 55°$) and (c) the material removal plane ($\phi = 0°$) during material removal at $t = 40$ s for Case 9.

dients beneath the laser spot may induce thermal stresses above a critical value. For this study, the relationship between L_ℓ and D_ℓ which provides adequate thermal softening and minimizes the probability of damaging the machined surface corresponds to $L_\ell \approx 0.8 D_\ell$.

Temperatures and temperature gradients throughout the workpiece increase with increasing laser beam power. Increased thermal softening is realized for increasing laser power, and is manifested by a decrease in the cutting forces and specific cutting energy [13].

The influence of representative variations in the absorptivity of the unmachined workpiece to laser irradiation ($\alpha_\ell \pm 6\%$), the emissivity of the unmachined and machined surface (ε, $\varepsilon_m + 8.4\%$), the convection heat transfer coefficient of the laser gas assist ($Nu_j \pm 14\%$), and the width of the primary shear zone ($s_{psz} + 100\%$, $s_{psz} - 50\%$) on the workpiece temperature distribution was studied numerically for the nominal operating condition. The values of the maximum temperature beneath the laser spot (T_{max}) and the minimum material removal temperature ($T_{mr,min}$) were only moderately influenced by variations in the values of α_ℓ ($\pm 120°C$, $\pm 52°C$). The values of T_{max} and $T_{mr,min}$ were not significantly influenced by an increase in the values of ε and ε_m ($-23°C$, $-19°C$) or by variations in the value of s_{psz} ($\pm 1°C$, $\pm 2°C$).

3. Conclusions

A transient, three-dimensional numerical model of LAM was constructed which includes a preheat phase, during which no workpiece translational motion occurs relative to the laser source. After preheating, material removal was initiated, thereby changing the workpiece geometry. Numerical calculations were completed at operating conditions corresponding to the LAM experiments detailed in a companion paper [1].

From the numerical model, it was found that thermal energy generation in the small primary shear zone ($\sim 10^{-5}$ mm^3) significantly increased surface temperatures near the material removal plane. While a majority of the generated thermal energy left the workpiece with the heated material (chips) due to the strong influence of circumferential advection near the

material removal location, conduction transported a portion of the thermal energy generated due to plastic deformation away from the primary shear zone and into the unmachined workpiece. Heating at the location corresponding to flank wear resulted in a slight local increase in the surface temperature. However, for the conditions of the present study, flank wear heating does not significantly influence the workpiece temperature distribution.

As in the case of heating without material removal [11], increases in the workpiece rotational speed decreased surface temperatures beneath the laser spot and decreased radial penetration of the temperature distribution. The amount of thermal energy generated within the primary shear zone leaving the workpiece with the heated material increased with increasing workpiece rotational speed, thereby decreasing the influence of conduction into the unmachined workpiece. Because the amount of energy deposition was fixed, the temperature distribution at axial locations removed from the laser was relatively uninfluenced by changes in workpiece rotational speed.

With increasing laser/tool translational velocity, and hence increasing axial advection, the reduction of the total laser energy deposition for a fixed laser power may preclude the attainment of a minimum material removal temperature corresponding to the softening temperature range of the YSiAlON glassy phase, while increasing the uniformity of the temperature distribution in the machined workpiece. Increases in the depth of cut provided a modest decrease in the minimum material removal temperature for a 50% increase in the material removal rate. Relative to nominal conditions, a decrease in the laser-tool lead distance decreases the amount of laser energy deposition within the unmachined workpiece, thereby decreasing the minimum material removal temperature. Conversely, if the laser-tool lead distance is increased, such that the laser no longer overlaps the chamfer, there is little change in the minimum material removal temperature, although there is a reduction in the average temperature over the material removal plane. For this study, it was found that a laser-tool lead distance corresponding to $L_\ell \approx 0.8 D_\ell$ provided the most favorable thermal conditions for LAM. Decreasing or increasing the beam diameter, for a fixed laser-tool lead, increases and decreases laser energy deposition at the unmachined workpiece surface, respectively. Decreasing the laser beam diameter also increases temperature gradients on the unmachined surface near and at radial locations just beneath the laser source. Far from the laser source, the workpiece temperature distribution is relatively unaffected by changes in the laser beam diameter. Temperatures and temperature gradients throughout the workpiece increase with increasing laser beam power.

Acknowledgements

The authors gratefully acknowledge the support of the National Science Foundation through Award Number 9400654-CTS.

References

[1] W. König, A.K. Zaboklicki, NIST Special Publication 847, National Institute of Science and Technology, 1993.
[2] D.P. Stinton, ORNL/TM-10791, Oak Ridge National Laboratory, 1988.
[3] H.G. Wobker, H.K. Tönshoff, NIST Special Publication 847, National Institute of Science and Technology, 1993.
[4] G. Chryssolouris, J. Shonbeck, W. Choi, P. Sheng, Advances in three-dimensional laser machining, in: E.S. Geskin (Ed.), Proceedings of the Winter Annual Meeting of the ASME, vol. PED-41, San Francisco, CA, 1989, pp. 1–7.
[5] K. Kawashimo, T. Yamada, Temperature distribution within a rotating cylindrical body heated and cooled locally on Its peripheral surface, Bulletin of the Japan Society of Mechanical Engineers 21 (152) (1978) 266–272.
[6] B. Gecim, W.O. Winer, Steady temperature in a rotating cylinder subject to surface heating and convective cooling, ASME Journal of Heat Transfer 106 (1984) 120–127.
[7] W.Y.D. Yuen, On the steady-state temperature distribution in a rotating cylinder subject to heating and cooling over its surface, ASME Journal of Heat and Mass Transfer 106 (1994) 578–585.
[8] W.Y.D. Yuen, The thermal boundary layer in a rotating cylinder subject to prescribed surface heat fluxes, International Journal of Heat and Mass Transfer 37 (4) (1994) 605–618.
[9] K. Koai, R. Damaschek, H.W. Bergmann, Heat transfer in laser hardening of rotating cylinders, in: Proceedings of the Winter Annual Meeting of the ASME, New Orleans, LA, vol. HTD-259, 1993, pp. 1–8.
[10] J.C. Rozzi, M.J.M. Krane, F.P. Incropera, Y.C. Shin, Numerical prediction of three-dimensional unsteady temperatures in a rotating cylindrical workpiece subjected to localized heating by a translating laser source, in: Proceedings of the International Mechanical Engineering Congress and Exhibition, San Francisco, CA, vol. HTD-317-2, 1995, pp. 399–411.
[11] J.C. Rozzi, F.P. Incropera, Y.C. Shin, Transient thermal response of a rotating cylindrical silicon nitride workpiece subjected to a translating laser heat source. Part II: parametric effects and assessment of a simplified model, ASME Journal of Heat Transfer 120 (4) (1998) 907–915.
[12] J.C. Rozzi, F.E. Pfefferkorn, F.P. Incropera, Y.C. Shin, Transient, three-dimensional heat transfer model for the laser assisted machining of silicon nitride: I. Comparison of predictions with measured surface temperature histories, International Journal of Heat and Mass Transfer 43 (2000) 1409–1424.
[13] J.C. Rozzi, Experimental and theoretical evaluation of the laser assisted machining of silicon nitride, Ph.D. Thesis, Purdue University, 1997.